Phosphorylation at S365 is a gatekeeper event that changes the structure of Cx43 and prevents down-regulation by PKC

Joell L. Solan,[1] Lucrecia Marquez-Rosado,[1] Paul L. Sorgen,[3] Perry J. Thornton,[1] Philip R. Gafken,[2] and Paul D. Lampe[1]

[1]Molecular Diagnostics Program and [2]Proteomics Shared Resource, Fred Hutchinson Cancer Research Center, Seattle, WA 98109
[3]University of Nebraska Medical Center, Omaha, NE 68198

Phosphorylation at unspecified sites is known to regulate the life cycle (assembly, gating, and turnover) of the gap junction protein, Cx43. In this paper, we show that Cx43 is phosphorylated on S365 in cultured cells and heart tissue. Nuclear magnetic resonance structural studies of the C-terminal region of Cx43 with an S365D mutation indicate that it forms a different stable conformation than unphosphorylated wild-type Cx43. Immunolabeling with an antibody specific for Cx43 phosphorylated at S365 shows staining on gap junction structures in heart tissue that is lost upon hypoxia when Cx43 is no longer specifically localized to the intercalated disk. Efficient phosphorylation at S368, an important Cx43 channel regulatory event that increases during ischemia or PKC activation, depends on S365 being unphosphorylated. Thus, phosphorylation at S365 can serve a "gatekeeper" function that may represent a mechanism to protect cells from ischemia and phorbol ester-induced down-regulation of channel conductance.

Introduction

Gap junctions are intercellular structures that facilitate direct communication among adjacent cells by allowing passage of ions and small metabolites (White and Paul, 1999; Saez et al., 2003; Sohl and Willecke, 2004; Laird, 2006). Vertebrate gap junctions, composed of integral membrane proteins encoded by the 21-member connexin gene family, are critically important in regulating embryonic development, coordinated contraction of excitable cells, tissue homeostasis, normal cell growth, and differentiation (Saez et al., 2003; Sohl and Willecke, 2004). Their functional importance has been shown by the linkage of connexin mutations to deafness and several diseases (Bergoffen et al., 1993; Gong et al., 1997; Kelsell et al., 1997; Laird, 2006) including oculodentodigital dysplasia, a disease linked to connexin43 (Cx43) mutations that can cause atrioseptal defects and arrhythmias (Paznekas et al., 2003).

Cx43, the most ubiquitously expressed connexin, is differentially phosphorylated at a dozen or more serine residues throughout its life cycle (Lampe and Lau, 2004; Solan and Lampe, 2005). Regulation of Cx43 may occur at many different stages, including the oligomerization of six connexin proteins into a hemi-channel or connexon, connexon transport to the plasma membrane, intercellular docking of connexons to form intercellular channels, condensation of hundreds to thousands of these channels into paracrystalline arrays (termed gap junctional plaques), gap junction channel gating, and turnover of plaques. There is correlative evidence that gap junctional communication and Cx43 levels may be controlled by phosphorylation of Cx43 at many of these steps; however, the mechanisms underlying these events have remained elusive.

Cx43 from cultured cells commonly demonstrates multiple electrophoretic isoforms when analyzed by SDS-PAGE: a faster migrating form (sometimes referred to as P0 or NP) that includes the nonphosphorylated isoform, and multiple slower migrating forms (sometimes termed P1 and P2) (Musil and Goodenough, 1991). After alkaline phosphatase treatment in vitro, the phosphorylated species collapse to the fastest migrating form, suggesting that phosphorylation is the primary covalent modification resulting in the conformational change detected in SDS-PAGE analysis. Studies investigating phosphorylation in normal rat kidney (NRK) cells showed that Cx43 acquired resistance to Triton X-100 and was found in gap junction plaques when it had been phosphorylated to the P2 isoform (Musil and Goodenough, 1991). P2 formation requires phosphorylation at S325, S328, and/or S330 (Lampe et al., 2006). Myocardial ischemia leads to unspecified Cx43 "dephosphorylation" events and loss of localization to

Correspondence to Paul D. Lampe: plampe@fhcrc.org

Abbreviations used in this paper: Cx43, connexin43; HSQC, ^{15}N-heteronuclear single-quantum correlation; LC, liquid chromatography; MS, mass spectrometry; NMR, nuclear magnetic resonance; NRK, normal rat kidney; WT, wild type.

The Journal of Cell Biology, Vol. 179, No. 6, December 17, 2007 1301–1309
http://www.jcb.org/cgi/doi/10.1083/jcb.200707060

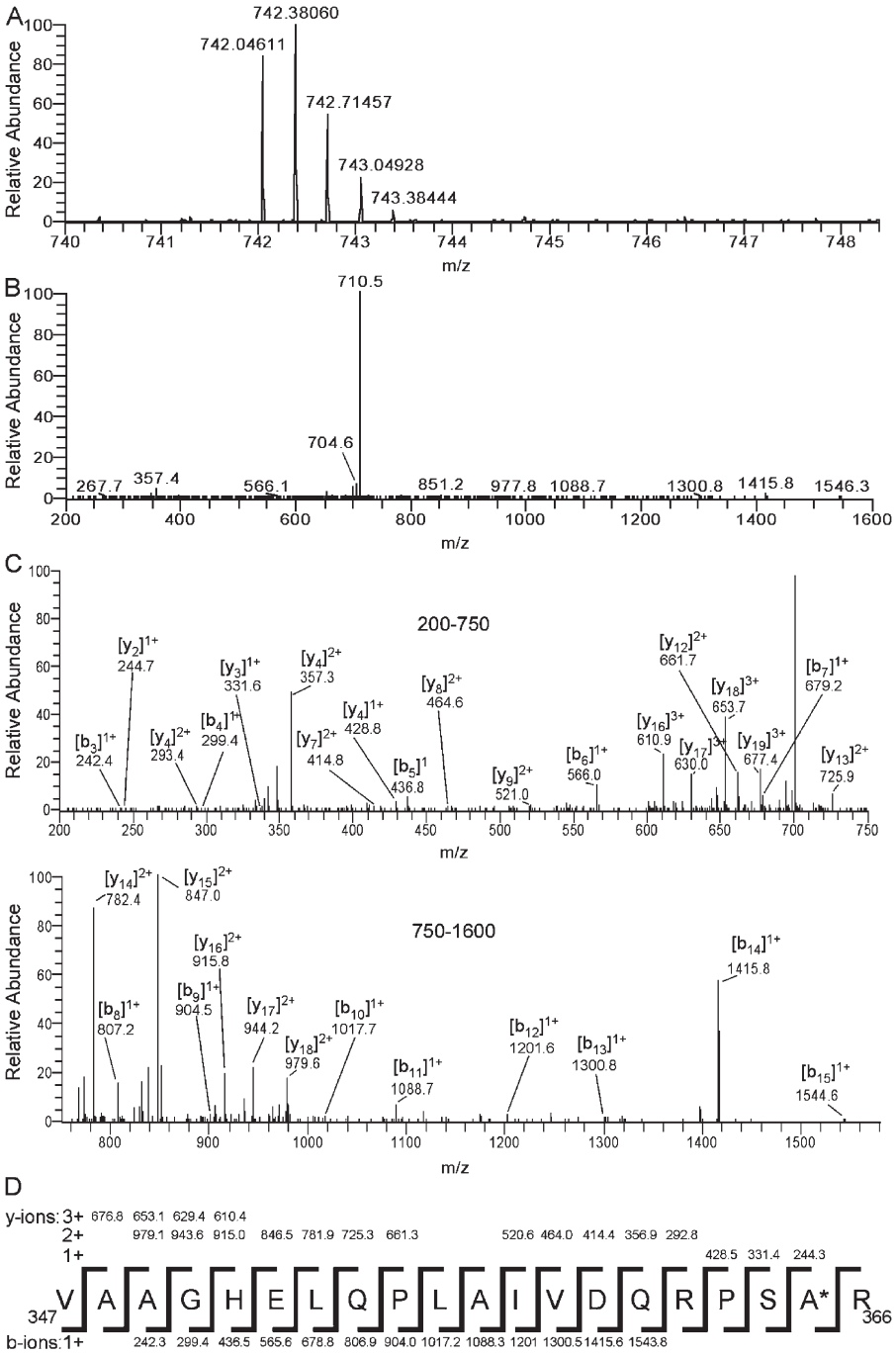

Figure 1. **LC/ESI MS/MS of a phosphorylated peptide from Cx43.** A gel band enriched for phosphorylated Cx43 was digested with trypsin and analyzed with an LTQ-FT mass spectrometer. (A) Chromatographic elution of the tryptic peptide mixture into the mass spectrometer revealed a peak at 26.02 min that contained a triply charged monoisotopic ion species (m/z 742.04611) that was suspected to be the peptide V347 to R366 of Cx43 containing a single phosphate group. (B) Tandem mass spectrometry (MS2) of this precursor ion species resulted in a fragmentation spectrum dominated by ion species m/z 710.5 that indicates the neutral loss of phosphoric acid (m/z 31.5) from the precursor. It is important to note that the deviation of m/z 1.2 from the expected value of m/z 32.7 for the neutral loss of a phosphate group is a result of the error associated with subtracting a low mass accuracy, average m/z value in B from the high mass accuracy, monoisotopic value in A. The difference in the two types of measurements is inherent with the mass measurement being performed with an LTQ-FT mass spectrometer. Tandem mass spectrometry (MS2) was performed on ion species m/z 742.04611 to generate the neutral loss species m/z 710.5 followed immediately by a second round of tandem mass spectrometry (MS3) on m/z 710.5. The resulting MS3 spectrum (C: split into 200–750 and 750–1600 m/z panels for legibility) showed numerous diagnostic b- and y-type ions to identify the Cx43 peptide as tryptic peptide V347 to R366. The observed fragment ions were compared with the expected fragment ions (D) showing that the peptide contains a dehydroalanine ("A*") at position 365 as a result of the neutral loss of phosphoric acid in the first round of tandem mass spectrometry. The site of dehydroalanine reveals that S365 as the site of phosphorylation within the peptide (note: only the expected fragment ions that were observed in the MS3 spectrum are indicated in D).

the intercalated disk, which likely contribute to contractile failure and arrhythmias (Beardslee et al., 2000; Schulz et al., 2003). Thus, uncharacterized phosphorylation events have been correlated with changes in Cx43 localization, inclusion in gap junction structures, and acquisition of Triton X-100 insolubility.

We have previously shown that Cx43 is phosphorylated at S368 in basal keratinocytes near the edge of a human wound, in heart tissue upon hypoxia, during S and G_2/M phases of the cell cycle, and upon treatment with phorbol esters (Lampe et al., 1998; Solan et al., 2003; Richards et al., 2004; Ek-Vitorin et al., 2006). Phosphorylation at S368 reduces the conductivity of the gap junction channel, potentially causing the formation of communication compartments (Ek-Vitorin et al., 2006). In this paper, we show that Cx43 is phosphorylated on S365 in homeostatic cells and that this event is required for formation of the P1 isoform. Structural studies of the C-terminal region of Cx43 with a S365D mutation, intended to mimic phosphorylation, indicate that this change generates a different stable conformation than unphosphorylated, wild-type Cx43. Preparation and use of an antibody specific for Cx43 only when it is phosphorylated at S365 showed that this phosphorylation event occurs on Cx43 present specifically in gap junction structures in cultured cells and in heart tissue. Phosphorylation at S365 was constitutive in heart tissue but absent during hypoxia when Cx43 loses its specific

localization at the intercalated disk and phosphorylation at S368 increases (Ek-Vitorin et al., 2006). Western, immunoprecipitation, and in vitro kinase studies show that efficient phosphorylation at S368 requires that S365 be unphosphorylated. We conclude that phosphorylation of Cx43 at S365 serves a "gatekeeper" function by causing a change in conformation that prevents PKC-dependent phosphorylation at S368 and subsequent changes in channel regulation.

Results

Determination of S365 as a site of phosphorylation in Cx43

Cx43 immunoprecipitated from confluent NRK cells was separated by SDS-PAGE and the bands representing phosphorylated Cx43 were excised and subjected to mass spectrometry (MS) sequence analysis. Tryptic peptide analysis by LC MS/MS revealed an ion species of m/z 742.04611 that was triply charged (Fig. 1 A, determined by the m/z difference of 0.333 between the isotopic peaks). A triply charged phosphorylated tryptic peptide of Cx43 with a m/z of 742.04645 would be predicted for the amino acids that span V347 to R366. Tandem mass spectrometry (MS2) of this ion species (Fig. 1 B) resulted in a spectrum dominated by a single ion species of m/z 710.5 that corresponded to the loss of m/z 31.6, suggesting the neutral loss of phosphoric acid. The other ion species in the MS2 spectrum were of very low intensity, making it difficult to interpret the amino acid sequence. A neutral-loss experiment was performed where ion species m/z 742.04611 was selected for MS2 and the resulting ion species m/z 710.5 was further selected for an additional round of fragmentation. The resulting MS3 spectrum (Fig. 1 C) showed abundant diagnostic fragment ions that verified the identity of the tryptic peptide V347-R366. Due to the neutral loss of a phosphate group, the phosphoserine would be converted to dehydroalanine. Analysis of the MS3 spectrum showed $[y_2]^{1+}$ = 244.7 and $[y_3]^{1+}$ = 331.6, which locate the dehydroalanine to position 365 (Fig. 1 C). In summary, S365 in Cx43 was determined to be phosphorylated based on three results: (1) the high mass accuracy between the ion species that was measured and that was predicted for phosphorylated V347-R366; (2) the production of a neutral-loss fragment during MS2 of V347-R366, indicating the loss of phosphoric acid; and (3) interpretation of an MS3 spectrum of the peptide undergoing neutral loss, indicating dehydroalanine at amino acid 365.

Antibody validation by Western blot and immunofluorescence

Because we found Cx43 to be significantly phosphorylated at S365, we prepared and immunoaffinity purified an antibody to Cx43 that only bound to S365 when it was phosphorylated (referred to as antibody pS365) by immunizing a rabbit with a synthetic phosphopeptide representing amino acids 361–369 with S365 being phosphorylated. To determine the specificity of the antibody, we transfected MDCK cells that do not express Cx43 (Jordan et al., 1999) with wild-type Cx43 or Cx43 containing the site-directed mutations S365A or S365D. After creation of stable lines by dilution cloning in antibiotic, we simultaneously probed

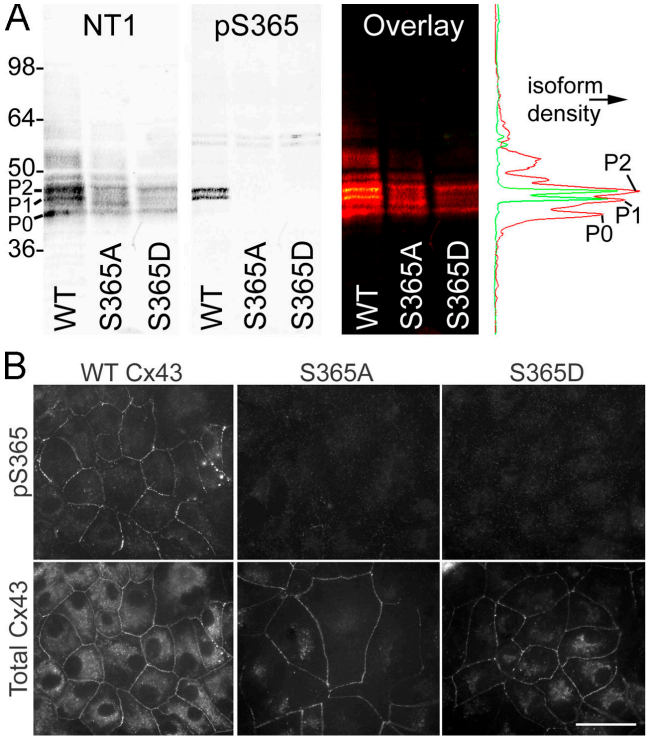

Figure 2. **pS365 is specific for Cx43 phosphorylated on S365, recognizes predominantly the P1 isoform of Cx43 and is found in apparent gap junction plaques.** (A) Western blot analysis of lysates from stably transfected MDCK cells, expressing wild type (WT), S365A or S365D mutant Cx43, were probed for total Cx43 (NT1) and with a polyclonal antibody generated to recognize Cx43 phosphorylated at S365. The phospho-antibody recognizes Cx43 in WT-expressing cells, but not when S365 is converted to alanine or aspartate. The faint bands in the 50–54-kD range are visible with multiple Cx43 antibodies, but we have been unable to identify the modification that leads to this migration shift. Overlay of NT1 (red) and pS365 (green) signals show that they are coincident. Densitometry on the individual isoforms (isoform density) shows that pS365 signal is highest in the P1 and P2 isoforms. The migration positions of molecular weight standards are indicated on the left in kD. (B) Immunofluorescence using pS365 and a monoclonal antibody for total Cx43 shows that pS365 resides predominantly in the plasma membrane (WT Cx43) and that the pS365 epitope is eliminated by conversion from serine to alanine or aspartate (S365A, S365D) (bar = 25 μm).

an immunoblot that contained cell lysates from each line with both a mouse monoclonal antibody prepared to the N-terminal region of Cx43 (NT1) and the pS365 antibody using a fluorescence-based co-labeling system. As shown in Fig. 2 A, the antibody to total Cx43 (NT1) bound to 41–44-kD (P0, P1, and P2) bands in the lane containing the lysate from wild-type cells (WT). The S365A cells exhibited the P0, P2, and a faint band intermediate between P0 and P1, but not a distinct P1 isoform. The S365D cells exhibited multiple faint bands migrating between P0 and P1. When the pS365 antibody labeling was examined in the other fluorescence channel, signal was only detected in the WT lane with a distinct prominent bands at P1and P2 as shown in the pS365 panel and in the overlay panel (NT1 [red] + pS365 [green]) of Fig. 2 A. Fig. 2 B shows co-labeled immunofluorescence of pS365 (top) and total Cx43 (bottom) in MDCK cells expressing wild-type, S365A, or S365D Cx43. The pS365 antibody only showed labeling of the WT-expressing cells, mostly at apparent junctional structures, whereas mutation to A or D eliminated pS365 labeling.

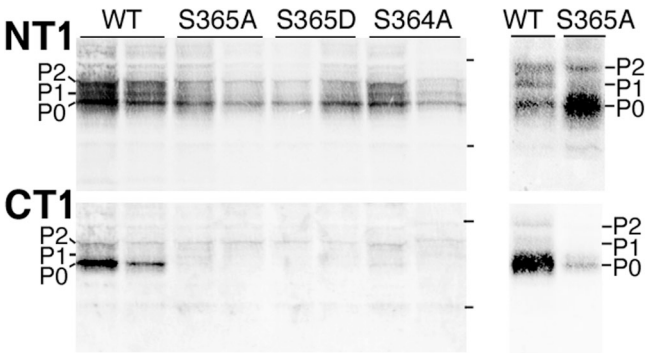

Figure 3. **Mutation of S365 eliminates the P1 isoform of Cx43.** Lysates from two separate stable cell lines expressing wild type (WT), S365A, S365D or S364A mutant Cx43 were probed for total Cx43 (NT1) and with an antibody that recognizes Cx43 containing unmodified S364 and S365 (CT1). WT and S364A make all three Cx43 isoforms, while neither S365A nor S365D make the P1 isoform. The two tick marks on the right side of the left panel indicate the position of 50- and 36-kD standards. The right panels show a comparison of WT and S365A Cx43 expressing cells with the latter being overloaded to show a lack of the P1 isoform.

The antibody to total Cx43 immunolabeled both apparent punctate junctional structures at cell–cell interfaces and cytoplasmic membranes in all three transfectants. Note that the pS365 antibody only labels a subset of the punctate gap junctional structures observed with the total Cx43 antibody and none of the cytoplasmic Cx43. The fact that mutation of S365 to A or D does not appear to affect the ability of Cx43 to transport to the membrane indicates that this phosphorylation event is probably not essential for gap junction assembly. We also performed dye microinjection experiments to see if the S365A mutant cells could participate in gap junctional communication. When the number of cells that received dye per microinjected cell was determined for S365A (31.6 ± 7.0; mean ± SEM) and wild-type Cx43 (30.7 ± 3.5) expressing clones, no statistical difference was observed.

Phosphorylation on S365 creates the P1 isoform

To study the role of S365 phosphorylation on the migratory isotypes of Cx43, we examined multiple clones of MDCK cell lines expressing Cx43 WT, S365A, and S365D. Because S365 is part of a diserine repeat (S364/S365) and S364 can be phosphorylated (TenBroek et al., 2001), we also examined how S364 affected Cx43 migration. When lysates from two separate clones for each Cx43 construct were examined by Western blot for total Cx43, we found that both S365 mutant clones made predominantly P0 and that neither made the P1 isoform of Cx43 (Fig. 3, NT1 panel). Even when the S365A clone was heavily overloaded relative to the wild type, no P1 was observed (Fig. 3, right panels). Although the S364A-containing cells made relatively more P0 than the wild type, they were capable of making the P1 and P2 isoforms (Fig. 3). We also examined these cells using an antibody generated in our lab, Cx43CT1 (CT1), which we have epitope mapped and found to be specific for Cx43 that is not phosphorylated at S364 or S365 (Sosinsky et al., 2007).

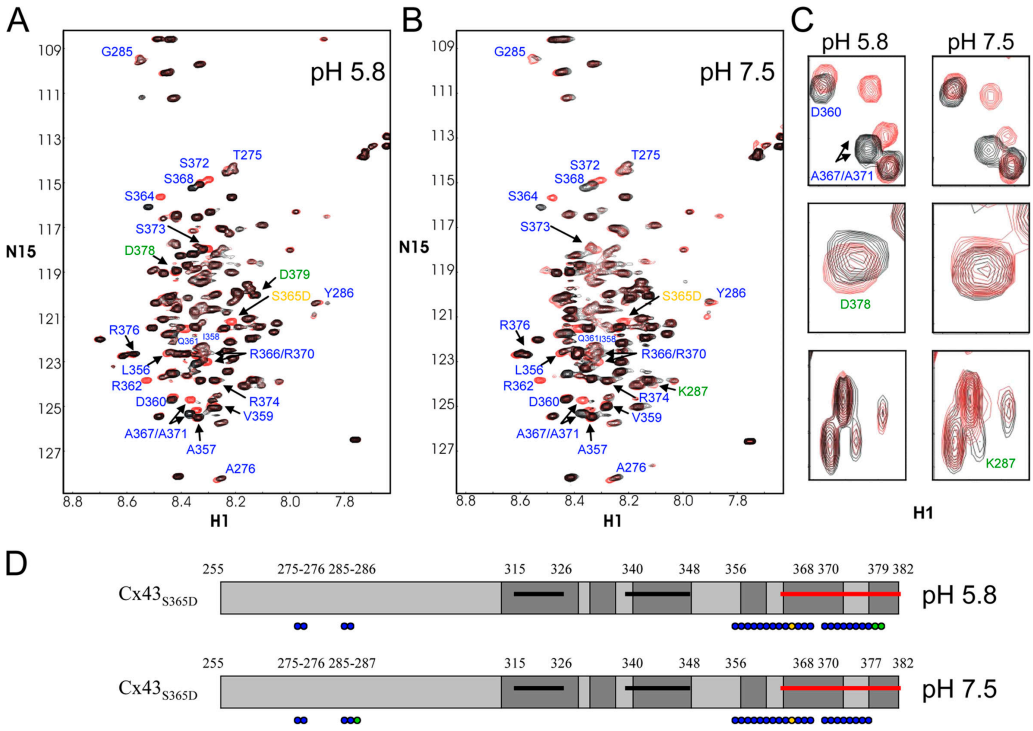

Figure 4. **NMR conformational analysis of wild-type and S365D mutant Cx43CT.** ^{15}N-HSQC spectra for wild-type Cx43CT (black) and S365D mutant (red) are presented in A (pH 5.8) and B (pH 7.5). C shows a close-up view of resonance peaks from A and B to illustrate residues that had clearly shifted at both pH 5.8 and 7.5 (top), that only shifted at pH 5.8 (middle), and that only shifted at pH 7.5 (bottom). D provides a summary of the residues affected by the S365D substitution at pH 5.8 and 7.5. The model and ^{15}N-HSQC spectra are encoded as follows: blue, common changes between pH 5.8 and 7.5, yellow, S365D point mutant; green, regions different between the two pHs; black line, helical domains (invariant between the two pHs); red line, residues affected by the ZO-1 PDZ-2 domain; and gray boxes, residues affected by the Cx43 cytoplasmic loop domain.

When this antibody is used to detect wild-type Cx43, we find that it does not recognize the P1 isoform of Cx43 (Fig. 3, CT1 panel), but it often recognizes a faint band that is an apparent subset of the P2 form. Note that this is consistent with the ability of the S365A and S365D mutants to make some P2. Mutation of either S364 or S365 ablated the ability of the CT1 antibody to recognize Cx43 (Fig. 3, CT1 panel), indicating that the serines themselves are important in creating the conformational epitope recognized by this antibody.

The structure of Cx43CT wild type vs. S365D mutant via NMR

We have recently used a combination of nuclear magnetic resonance (NMR) and mirror resonance technology to characterize the structure of the CT of Cx43 (Cx43CT) and assign backbone and side chain resonance values for most of the residues from 255–382 (Duffy et al., 2002; Sorgen et al., 2004b). These studies indicated a pH-dependent shift in the ability of Cx43CT to interact with itself, with the cytoplasmic loop of Cx43, and other interacting proteins (Duffy et al., 2002; Sorgen et al., 2002, 2004a,b). Here, we used similar ^{15}N-heteronuclear single-quantum correlation (HSQC) experiments to compare the structure of wild-type and a mutant version of Cx43CT that only varied by the substitution of S365 with aspartic acid to mimic phosphorylation at that site (Fig. 4). The ^{15}N-HSQC is a two-dimensional NMR experiment in which each amino acid (except proline) gives one signal (or chemical shift) that corresponds to the N–H amide group. These chemical shifts are sensitive to the chemical environment, and even small changes in structure and/or dynamics can change the chemical shift of an amino acid. At pH 5.8, this substitution (Fig. 4 A, yellow) affected the resonance peaks of residues T275-A276, G285-Y286, L356-S368, and R370-D379 (shown in blue, except D378 and D379 [green]). A blown-up view shows the extensive shifts of D360 and A367/A371 (Fig. 4 C, top left) and D378 (middle left). At pH 7.5, T275-A276, G285-K287, L356-S368, and R370-R376 also showed different resonance values between the wild-type and S365D mutant. Although most of these shifts were very comparable to pH 5.8 values, K287 changes at pH 7.5 but D378-D379 does not (areas highlighted in green in A and B, and their difference emphasized in the bottom four sections of C). In general, the residues closer to the mutation had dramatic shifts, indicating the formation of a stable conformation different than the wild type, while the others were more subtle. We conclude that the S365D mutation has a dramatic effect on the structure at either pH with slight differences between the two.

S365 is constitutively phosphorylated in heart and becomes dephosphorylated during hypoxia

We examined S365 phosphorylation using a model of ischemia in mouse heart. Cx43 in normal heart is concentrated in gap junction plaques at the intercalated disk (Fig. 5), as has been shown in numerous other studies (Jain et al., 2003; Schulz et al., 2003). When hypoxia is induced, Cx43 is redistributed to the lateral edges so that it is no longer concentrated at the intercalated disk (Fig. 5; Beardslee et al., 2000; Schulz et al., 2003; Ek-Vitorin et al., 2006). We examined Cx43 phosphorylation at S365, as detected with the pS365 antibody, in heart before and after hypoxia. The pS365 antibody showed extensive labeling at the intercalated disk in control heart that was lost upon hypoxia. We have previously reported that phosphorylation on S368 was actually increased during hypoxia (Ek-Vitorin et al., 2006), as also shown in Fig. 5 (bottom panels). Analysis of 8 fields of heart tissue for each condition indicated a 1.8-fold increase in pS368 staining at intercalated disk upon hypoxia that was statistically different from the control ($P = 0.04$). Because dephosphorylation is a key event during ischemia, we investigated the potentially antagonistic relationship between phosphorylation at S365 and S368.

Phosphorylation at S365 prevents phosphorylation at S368

Treatment of cells with phorbol esters has been shown to increase the phosphorylation of Cx43 at S368 (Lampe et al., 2000;

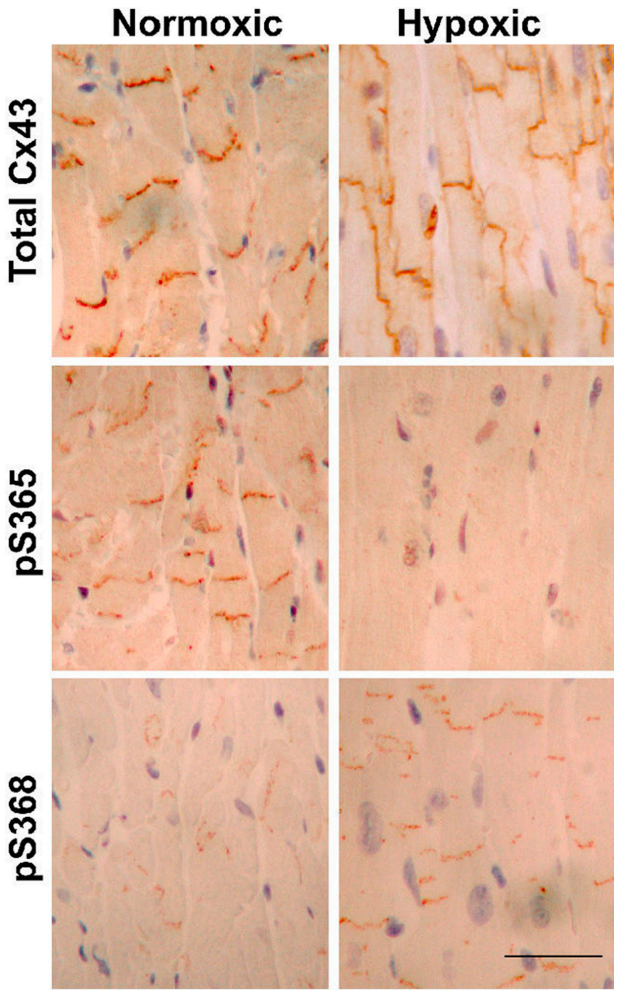

Figure 5. **Differential phosphorylation of Cx43 localized at intercalated disks vs. lateral edges of myocytes in the normoxic and ischemic heart.** The localization of total Cx43, pS65-Cx43, and pS368 in normoxic and hypoxic heart is shown. Note the increase in total Cx43 at the lateral edges of the myocytes and loss from the intercalated disk of the ischemic heart. Cx43 was not detectably phosphorylated at S365 in the hypoxic heart, but phosphorylation at S368 was increased mainly in the intercalated disk region (bar = 20 μm).

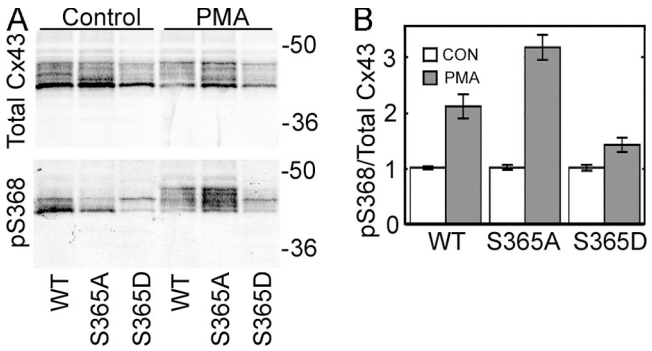

Figure 6. **Conversion of S365 to alanine enhances, while aspartate inhibits PMA-activated phosphorylation of S368.** (A) Western blot of cell lysates from wild-type Cx43 (WT), S365A, and S365D cells treated with 100 nM PMA for 30 min (PMA) or not (CON) were probed for total Cx43 (NT1) and Cx43 phosphorylated on S368 (pS368). The migration positions of molecular weight standards are indicated on the right in kD. (B) Signals were quantified and expressed as a ratio of pS368 over NT1. Shown are results of three experiments using three separate clones (nine total measurements) for each construct. Values were normalized to control for each clone and error bars represent SEM. Western blot is representative, showing a single clone for each construct.

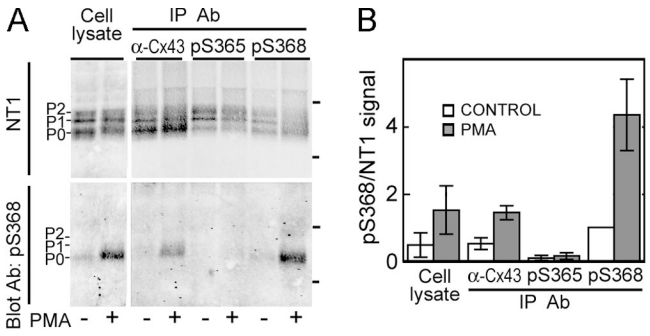

Figure 7. **Cx43 phosphorylated on S365 is not phosphorylated on S368.** (A) Western blot of Cx43 immunoprecipitated from NRK cells treated with 100 nM PMA for 30 min (+) or untreated (−). Cx43 from lysates or Cx43 immunoprecipitated from cell lysates using antibodies to total Cx43 (α-Cx43), pS365, or pS368 were probed for total Cx43 (NT1, top) and Cx43 phosphorylated on S368 (pS368, bottom). The two tick marks on the right side indicate the position of 50- and 36-kD standards. (B) Signals were quantified and expressed as a ratio of pS368 over NT1 normalized to a value of 1 for the untreated sample immunoprecipitated and immunoblotted for pS368 to allow comparison for five separate experiments (mean ± SEM).

Solan et al., 2003), so MDCK cells expressing wild-type (WT), S365A, or S365D Cx43 were treated with PMA to examine phosphorylation levels at S368 compared with control levels. We found that control levels of pS368 antibody binding were similar between WT and S365A-expressing cells, but pS368 levels were reduced in S365D cells (Fig. 6). Furthermore, PMA treatment led to more than a two- and three-fold increase in S368 phosphorylation in the WT and S365A cells, respectively, whereas there was only a 0.3-fold increase in S365D cells. These results indicate that having a negative charge at S365 inhibited phosphorylation at S368 and mutation of S365 to a neutral, nonphosphorylatable residue increased the ability of PMA to stimulate phosphorylation at S368. However, these results cannot definitively argue the interdependence of the phosphorylation events because conversion to D does not exactly replicate addition of a phosphate, and a low level of phosphorylation at S368 was detected in the S365D mutant.

To further address this question, we looked specifically at these Cx43 phosphoforms, using NRK cells that endogenously express Cx43. Immunoprecipitations were performed using three different polyclonal antibodies, pS365, pS368, and an anti-Cx43 antibody (α-Cx43) that recognizes all three isoforms of Cx43. Western blots of these lysates were simultaneously probed with monoclonal NT1 (Fig. 7 A, top) and pS368 (Fig. 7 A, bottom) and detected in separate channels. Note that pS365 antibody immunoprecipitated predominantly the P1 and P2 isoforms, but a small fraction of immunoprecipitated Cx43 migrated at P0 or between P0 and P1. The pS365 antibody could be slightly less specific under immunoprecipitation conditions. However, it is also possible that some dephosphorylation occurs during the immunoprecipitation protocol, leading to the minor amounts of apparent P0 after SDS-PAGE. In both the cell lysate and α-Cx43 immunoprecipitate, pS368 was detectable mostly in the PMA-treated cells (PMA+), migrating primarily at the P0 position and nearly absent from control cells (PMA−). When expressed as pS368 signal over NT1 signal (Fig. 7 B), a 3–4.3-fold increase was observed upon PMA treatment for cell lysates and lysates immunoprecipitated with α-Cx43 or pS368. Cell lysates immunoprecipitated with pS365 showed little pS368 or P0 regardless of treatment, and these values were statistically different than those for both the α-Cx43 or pS368 immunoprecipitates ($P < 0.01$), consistent with phosphorylation of S365 preventing phosphorylation on S368. Collectively, these mutant and immunoprecipitation data indicate that phosphorylation at S365 prevents phosphorylation at S368 in response to PMA.

PMA increases PKC activity and PKC has been shown to phosphorylate Cx43 at S368 in vitro (Saez et al., 1997; Lampe et al., 2000). Therefore, we wanted to see if a negative charge at S365 directly inhibited the ability of PKC to phosphorylate Cx43. Wild-type and S365D GST-Cx43CT fusion proteins were phosphorylated with PKC and probed with the pS368 antibody. The wild-type version of the protein was efficiently phosphorylated, whereas the mutant was not, as shown in Fig. 8 A. To be more quantitative about the difference and to ensure that the affinity of the pS368 antibody was not affected by the mutation at S365, we also performed the reaction with γ-[^{32}P]ATP. Autoradiography (Fig. 8 B) and excision of the bands and scintillation counting indicated that PKC phosphorylated the wild type 4.3-fold more efficiently than the S365 Cx43CT ($n = 4$, significant at $P < 0.0001$). We conclude that phosphorylation at S365 dramatically reduces the efficiency of PKC-dependent phosphorylation at S368.

Discussion

In this manuscript, we have presented the following evidence that phosphorylation of Cx43 at S365 is a key regulatory event: Cx43 is phosphorylated on S365 in homeostatic cells. NMR structural studies of the C-terminal region of Cx43 with a S365D mutation indicate that it forms a different stable conformation

than unphosphorylated wild type Cx43. An antibody specific for Cx43 only when it is phosphorylated at S365 showed that this phosphorylation event occurs on Cx43 present in gap junction structures and in heart tissue at intercalated disks. Phosphorylation at S365 was constitutive in heart tissue and lost upon hypoxia when the specific localization of Cx43 to the intercalated disk was also lost. Phosphorylation at S368, on the other hand, increased in heart upon 30 min of hypoxia. Phosphorylation at S368 was dramatically reduced when S365 was phosphorylated arguing that S365 dephosphorylation likely precedes S368 phosphorylation during hypoxia. PKC-dependent phosphorylation of S368 was dramatically reduced by mimicking phosphorylation at S365 with a S365D mutation. We conclude that phosphorylation of Cx43 at S365 serves a gatekeeper function by causing a change in conformation that allows maintenance of gap junctional communication.

We also present evidence that S365 phosphorylation is necessary for the full SDS-PAGE migration shift from P0 to P1: S365A mutants are not capable of making the P1 isoform (Figs. 2 and 3). The CT1 antibody, which we have epitope mapped to unphosphorylated S364/S365 (Sosinsky et al., 2007), does not recognize P1 or the S365A and S365D mutants (Fig. 3). Our pS365 antibody has a strong preference for the P1 and P2 isoforms, especially in a Western assay but also upon immunoprecipitation (Figs. 2 and 7). The pS365 antibody binds only to junctional Cx43 in immunofluorescence (Figs. 2 and 5). The S365D mutation leads to a discernable conformational change by NMR (Fig. 4); because addition of phosphate (i.e., 80 D) cannot account for the 2–3-kD apparent shift in molecular weight observed between P0 and P1, the conformational change could be responsible for the shift. Other phosphorylation events may also play a role in the shift, but we conclude that phosphorylation at S365 is necessary.

Phosphorylation of Cx43 at S364, S365, S368, S369, and S373 has been reported in response to increased cAMP levels (TenBroek et al., 2001; Yogo et al., 2002, 2006). In this paper, we found that phosphorylation at S365 occurred in homeostatic cells. Thus, we consider phosphorylation on S365 a "constitutive" event in the Cx43 "life cycle". We were surprised that substitution of S365 with aspartic acid had such dramatic effects on the solution structure of the C-terminal region of Cx43. Not only were residues L356-D379 affected, but 275-A276 and G285-Y286—almost 100 residues upstream—were also affected. We can only speculate that the C-terminal region interacts with residues in the 275–286 range, affecting its structure. Interestingly, some of the Cx43CT residues affected by the S365D substitution overlap with the residues previously identified to be affected by the interaction with the Cx43 cytoplasmic loop and the ZO-1 PDZ-2 domains (Sorgen et al., 2004a), which suggests the binding affinity of both domains may be affected by S365 phosphorylation.

In heart, Cx43 is localized to intercalated disks where it supports the longitudinal and transverse spread of the action potential, resulting in coordinated contraction. Myocardial ischemia/hypoxia leads to Cx43 dephosphorylation and loss of Cx43 localization to the intercalated disk, which likely contributes to apoptosis, contractile failure, and arrhythmias (Beardslee et al., 2000; Schulz et al., 2003). Ischemic preconditioning, or exposure of the heart to a brief period(s) of ischemia (e.g., 2–5 min) followed by reperfusion, before a more prolonged ischemic period (i.e., 30 min or more) protects the heart against necrosis and fatal arrhythmias (Cohen et al., 2000; Jain et al., 2003; Schulz et al., 2003). PKC is activated during preconditioning and appears to be necessary for protection against injury during the subsequent prolonged ischemic period. Because cardiac ischemia/hypoxia causes PKC activation, unidentified Cx43 dephosphorylation events, Cx43 relocalization (Beardslee et al., 2000; Schulz et al., 2003), and PKC-dependent phosphorylation of Cx43 at S368, the interrelationship of Cx43 phosphorylation at S365 and S368 will likely prove to be important in ischemia and preconditioning. Furthermore, because phosphorylation at S368 is regulated by tumor promoting agents, is controlled during the cell cycle, and is developmentally regulated (Lampe et al., 2000; Solan et al., 2003; King and Lampe, 2005), this gatekeeper role for S365 phosphorylation may be critical for growth control.

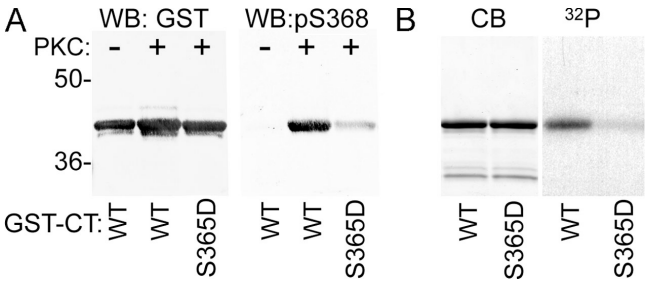

Figure 8. **PKC can efficiently phosphorylate wild type, but not the S365D mutant Cx43.** PKC was used to phosphorylate wild-type (WT) and S365D mutant GST-Cx43CT in vitro and the proteins were separated by SDS-PAGE. (A) The level of S368 phosphorylation was determined in a Western blot with pS368 antibody (WB:pS368) and consistent loading was shown with an antibody to GST (WB:GST). The migration positions of molecular weight standards are indicated on the left in kD. (B) The level of phosphorylation was determined directly by incorporation of ^{32}P from radiolabeled ATP and autoradiography (^{32}P panel). Consistent loading is shown in the panel showing the Coomassie blue–stained gel (CB panel).

Materials and methods

Antibodies, cDNA constructs, and other reagents

All general chemicals, unless otherwise noted, were purchased from Fisher Scientific. Mouse anti-Cx43 antibodies, Cx43CT1 and Cx43IF1, were prepared against amino acids 360–382 of Cx43 and antibody Cx43NT1 against amino acids 1–20 (Cx43NT1) of Cx43 (described in Cooper and Lampe, 2002; Lampe et al., 2006; Sosinsky et al., 2007) at the Fred Hutchinson Cancer Research Center Hybridoma Development Facility (Seattle, WA). The pS368 antibody was custom prepared and affinity purified by 21st Century Biochemicals. A rabbit antibody against Cx43 was purchased from Sigma-Aldrich and a similar rabbit antibody (α-Cx43) produced to the peptide representing A367-I382 of Cx43 was a gift of Alton Boynton (Northwest Biotherapeutics, Bothell, WA; Hossain et al., 1998). We made a rabbit anti-pS365-Cx43 antibody by custom commercial preparation (ProSci, Inc.; 13-wk schedule) against a synthetic peptide that was phosphorylated at S365 (CQRPS(pS)RASS-amide) and that we linked via the N-terminal cysteine to maleimide-activated KLH (Pierce Chemical Co.) according to manufacturer's instructions. Phosphospecific antibody was affinity purified essentially identically to our previously published method (Lampe et al., 2006). In brief, this involved passing the serum first over a column prepared with the nonphosphorylated peptide, followed by a phosphopeptide column and elution of the phosphospecific antibody.

Serine-to-alanine mutations at S364 and S365 were made using the GeneTailor site-directed mutagenesis system (Invitrogen) on full-length Cx43 that had been cloned into the mammalian expression vector pIREShyg (Clonetech Laboratories, Inc.). A serine-to-aspartic acid mutation at S365 was similarly performed on GST-Cx43CT (the C-terminal region of Cx43, amino acids 255–382 linked to the C terminus of GST), and the wild-type and mutant protein were expressed and purified as previously described for the wild-type version (Duffy et al., 2002).

Cell line maintenance and transfection

NRK-E51 (American Tissue Culture Collection; Manassas, VA) and MDCK cells were cultured in DME (Mediatech) supplemented with 10% FBS and antibiotics in a humidified 5% CO_2 environment. Wild-type and mutant Cx43 were electroporated into the MDCK cell lines via a Nucleofector apparatus (Amaxa Biosystems). Stably transfected clones were isolated with cloning rings and selected with hygromycin (200 μg/ml).

Identification of S365 as a phosphorylated residue

Ten 150-cm plates of NRK cells were grown to confluency and lysed in PBS containing phosphatase/protease inhibitors (50 mM NaF, 500 μM Na_3VO_4, 2 mM PMSF, 1× Roche Complete protease inhibitors) and 1% Triton X-100. After centrifugation at 30,000 *g* for 30 min at 4°C, the pellet was resuspended in RIPA buffer (25 mM Tris-HCl, 100 mM NaCl, 10 mM EDTA, and protease/phosphatase inihibitors) containing 0.5% Triton X-100, 0.5% sodium deoxycholate, and 0.1% SDS, and pre-cleared with protein A beads. Cx43 was immunoprecipitated with monoclonal Cx43CT1 and Cx43IF1 antibodies using protein A beads. The immunoprecipitate was subjected to SDS-PAGE (10% polyacrylamide) and protein bands were silver stained. Bands corresponding to phosphorylated Cx43 were excised from the gel and the silver stain was removed by incubation with equal volumes of 30 mM $K_4Fe(CN)_6$ and 100 mM $Na_2S_2O_3$ for 5 min, followed by several washes with 100 mM NH_4CO_3 until the gel slices were clear. Destained gel slices were subjected to in-gel tryptic digestion as previously described (Shevchenko et al., 1996) and the resulting peptide mixtures were desalted using a microC18 ZipTip and taken to dryness. Samples were then resuspended in 5 μl of 0.1% formic acid and analyzed by liquid chromatography coupled to electrospray ionization tandem mass spectrometry (LC/ESI MS/MS) with a nano2D LC (Eksigent Technologies) coupled to an LTQ-FT mass spectrometer (ThermoElectron Corporation) as previously described (Yi et al., 2003). Data were collected in a data-dependent mode in which a high mass resolution/high mass accuracy scan (in the FT part of the instrument) was followed by low resolution/low mass accuracy MS/MS scans (in the LTQ part of the instrument) of the three most abundant ions from the preceding MS scan. The FT part of the instrument was set at a target resolution of 100,000 at m/z 400, an AGC target value of 1e6, and a maximum ion time of 1,500 ms, while the ion trap was set to a MSn AGC target value of 1e4 and a MSn maximum ion time of 100 ms. The data-dependent method triggered a MS3 (MS/MS/MS) analysis on a MS2 (MS/MS) ion species if a MS2 ion species differed from the precursor ion species by m/z 98.0, 49.0, or 32.7, the neutral loss of phosphoric acid for a singly, doubly, or triply charged ion species, respectively. Normalized collision energy of 35% and isolation widths of 2.0 were used for both MS2 and MS3 events. Dynamic exclusion was enabled with a repeat count of 2, a repeat duration of 30 s, an exclusion duration of 60 s, and an exclusion mass width of 1.5.

Immunoblotting and immunoprecipitation

For whole cell extracts, cells were lysed in sample buffer containing 50 mM NaF, 500 μM Na_3VO_4, 2 mM PMSF, and 1× Complete protease inhibitor (Roche), and cellular proteins were separated by SDS-PAGE (10% polyacrylamide). For immunoprecipitation, cells were rinsed in PBS and lysed on ice in RIPA buffer (25 mM Tris-HCl, 100 mM NaCl, 10 mM EDTA, 50 mM NaF, 500 μM Na_3VO_4, 0.5% Triton X-100, 0.5% deoxycholate, 2 mM PMSF, and 1× Complete protease inhibitors). Cx43 was immunoprecipitated using pS365, pS368, and α-Cx43 antibodies by incubation with cell lysate for 2 h, followed by incubation with protein A for 1 h at 4°C. After several washes in RIPA buffer, Cx43 was eluted in 2× Laemmli sample buffer and separated by SDS-PAGE. Protein was transferred to nitrocellulose, the membrane was blocked, and antibodies were incubated as previously indicated (Lampe et al., 2006). pS365 and pS368 were detected with AlexaFluor 680 or IRDye800 anti–rabbit antibody, CT1 antibody (IgG2a) with fluorescent dye-labeled isotype specific secondary antibody (AlexaFluor680 goat anti–mouse IgG2a (Molecular Probes, Inc.), and NT1 (IgG1) with IRDye800 donkey anti–mouse IgG1 (Rockland Immunochemicals) (all extensively cross-reacted against other species) and directly quantified using the Li-Cor Biosciences Odyssey infrared imaging system and associated software. Images were converted from16-bit to 8-bit images after maximizing the dynamic range of pixel intensity using the "Levels" function in Adobe Photoshop. Most images (except Fig. 2 A overlay) were inverted to present them in the conventional black-on-white manner.

Immunofluorescence and immunostaining

Cells were washed twice in PBS, fixed in cold methanol/acetone (50:50) for 1 min, and blocked for 1 h in 1% BSA in PBS. Cells were incubated with anti-Cx43 antibody (pS365 antibody, Cx43CT1, and/or Cx43IF1) in blocking solution for 1 h. After several PBS washes, the cultures were incubated with Alexa 594–conjugated goat anti–rabbit antibody and/or Alexa 488–conjugated goat anti–mouse antibody for 30–60 min and counterstained with DAPI (Molecular Probes), followed by several washes in PBS. The coverslips were mounted onto slides with DABCO anti-fade medium (25 mg/ml of 1,4-Diazobicyclo-(2,2,2)octane [Sigma-Aldrich] diluted in Spectroglycerol [Kodak] and 10% PBS, pH 8.6) and viewed with a Nikon Diaphot TE300 fluorescence microscope, equipped with a 40× (1.3 NA) Plan Fluor oil objective; images were collected with a Princeton Instruments −20°C cooled digital camera driven by an attached PC and MetaMorph imaging software.

Immunohistochemistry

All mouse studies were conducted under Institutional Animal Care and Use Committee approval (FHCRC). Inbred mice (4 mo of age in a FVB/N: C57BL6 background) were anaesthetized (avertin, 0.83 mg/g body weight), hearts excised and placed either in cold PBS (with 1.8 mmol/L calcium, glucose free) for 30–60 s (control group) or incubated without coronary perfusion in warm (37°C), non-oxygenated PBS for 30 min ("hypoxia group") (Ek-Vitorin et al., 2006). Formalin-fixed heart tissue was processed, sectioned, immunostained, and microscopically analyzed as previously described (King and Lampe, 2004). In brief, tissue sections were deparaffinized, antigen retrieved, blocked, and detected using rabbit anti-Cx43, pS365, or pS368. Slides were washed and incubated with a biotinylated anti–rabbit secondary antibody (1:250) and detected with ABC-avidin/biotin conjugate (Vectastain; Vector Laboratories). 24-bit color images were collected using a Nikon Coolpix 990 digital camera attached to a Nikon Eclipse E400 microscope equipped with a 10× Plan Fluor objective (0.3 NA). We quantified the extent of pS368 staining at intercalated discs in control and hypoxic heart sections using MetaMorph 7.0 (Molecular Devices). Using the "Set Color Threshold" function, we selected the pS368 staining using the "Set by Example" function. The same Threshold values were used for all images analyzed. The integrated intensity of the thresholded pixels was measured. This value was normalized to the total area of tissue in each image. The area was determined by drawing a region around the tissue and measuring within this region. Eight images were analyzed per condition and a two-sided *t* test was performed.

Nuclear magnetic resonance

NMR data were acquired at 7°C using a 600-MHz Varian INOVA NMR spectrometer fitted with a cryoprobe at the University of Nebraska Medical Center's NMR Shared Resource Facility. Gradient-enhanced two-dimensional ^{15}N-HSQC experiments (Kay et al., 1992) were used to observe all backbone amide resonances in ^{15}N-labeled Cx43CT wild-type and S365D mutant Cx43CT. Data were acquired with 1024 complex points in the direct dimension and 128 complex points in the indirect dimension. Sweep widths were 10,000 Hz in the proton dimension and 2,500 Hz in the nitrogen dimension. NMR spectra were processed using NMRPipe (Delaglio et al., 1995) and analyzed using NMRView (Johnson and Blevins, 1994).

In vitro phosphorylation

Wild-type or S365D mutant GST-Cx43CT attached to glutathione beads was phosphorylated with 10 units of PKC (Phospho Solutions) in 10 mM $MgCl_2$, 50 mM NaCl, 40 mM Tris-HCl, pH 7.5, and 100 μM γ-[^{32}P]ATP (BLU002; Perkin Elmer) for 10 min. After three washes in PBS, sample buffer including 5% β-mercaptoethanol was added, samples were separated by SDS-PAGE, and the gel was stained with Coomassie blue. The stained gel was scanned in the Li-Cor scanner to determine protein loads, subjected to autoradiography using Hyperfilm (Amersham Biosciences), and the bands were subsequently excised to allow the radioactivity to be quantified in a scintillation counter (Beckman Coulter) and a two-sided *t* test was performed.

We thank Denis Bouvier for performing the NMR experiments.

These studies were supported by grants from the National Institutes of Health: GM055632 (P.D. Lampe) and GM072631 (P.L. Sorgen). Partial

funding for the LTQ-FT mass spectrometer used in this work was generously provided by the M.J. Murdock Charitable Trust.

Submitted: 9 July 2007
Accepted: 15 November 2007

References

Beardslee, M.A., D.L. Lerner, P.N. Tadros, J.G. Laing, E.C. Beyer, K.A. Yamada, A.G. Kleber, R.B. Schuessler, and J.E. Saffitz. 2000. Dephosphorylation and intracellular redistribution of ventricular connexin43 during electrical uncoupling induced by ischemia. *Circ. Res.* 87:656–662.

Bergoffen, J., S.S. Scherer, S. Wang, M. Oronzi Scott, L.J. Bone, D.L. Paul, K. Chen, M.W. Lensch, P.F. Chance, and K.H. Fishbeck. 1993. Connexin mutations in X-linked Charcot-Marie-Tooth disease. *Science.* 262:2039–2042.

Cohen, M.V., C.P. Baines, and J.M. Downey. 2000. Ischemic preconditioning: from adenosine receptor to KATP channel. *Annu. Rev. Physiol.* 62:79–109.

Cooper, C.D., and P.D. Lampe. 2002. Casein kinase 1 regulates connexin43 gap junction assembly. *J. Biol. Chem.* 277:44962–44968.

Delaglio, F., S. Grzesiek, G.W. Vuister, G. Zhu, J. Pfeifer, and A. Bax. 1995. NMRPipe: a multidimensional spectral processing system based on UNIX pipes. *J. Biomol. NMR.* 6:277–293.

Duffy, H.S., P.L. Sorgen, M.E. Girvin, P. O'Donnell, W. Coombs, S.M. Taffet, M. Delmar, and D.C. Spray. 2002. pH-dependent intramolecular binding and structure involving Cx43 cytoplasmic domains. *J. Biol. Chem.* 277:36706–36714.

Ek-Vitorin, J.F., T.J. King, N.S. Heyman, P.D. Lampe, and J.M. Burt. 2006. Selectivity of Connexin 43 Channels Is Regulated Through Protein Kinase C-Dependent Phosphorylation. *Circ. Res.* 98:1498–1505.

Gong, X., E. Li, G. Klier, Q. Huang, Y. Wu, H. Lei, N.M. Kumar, J. Horwitz, and N.B. Gilula. 1997. Disruption of alpha3 connexin gene leads to proteolysis and cataractogenesis in mice. *Cell.* 91:833–843.

Hossain, M.Z., P. Ao, and A.L. Boynton. 1998. Rapid disruption of gap junctional communication and phosphorylation of connexin43 by platelet-derived growth factor in T51B rat liver epithelial cells expressing platelet-derived growth factor receptor. *J. Cell. Physiol.* 174:66–77.

Jain, S.K., R.B. Schuessler, and J.E. Saffitz. 2003. Mechanisms of delayed electrical uncoupling induced by ischemic preconditioning. *Circ. Res.* 92:1138–1144.

Johnson, B., and R. Blevins. 1994. NMR VIEW—a computer-program for the visualization and analysis of NMR data. *J. Biomol. NMR.* 4:603–614.

Jordan, K., J.L. Solan, M. Dominguez, M. Sia, A. Hand, P.D. Lampe, and D.W. Laird. 1999. Trafficking, assembly and function of a connexin43-green flourescent protein chimera in live mammalian cells. *Mol. Biol. Cell.* 10:2033–2050.

Kay, L.E., P. Keifer, and T. Saarinen. 1992. Pure absorption gradient enhanced heteronuclear single quantum correlation spectroscopy with improved sensitivity. *J. Am. Chem. Soc.* 114:10663–10665.

Kelsell, D.P., J. Dunlop, H.P. Stevens, N.J. Lench, J.N. Laing, G. Parry, R.F. Mueller, and I.M. Leigh. 1997. Connexin 26 mutations in hereditary non-syndromic sensorineural deafness. *Nature.* 387:80–83.

King, T.J., and P.D. Lampe. 2004. The gap junction protein connexin32 is a mouse lung tumor suppressor. *Cancer Res.* 64:7191–7196.

King, T.J., and P.D. Lampe. 2005. Temporal regulation of connexin phosphorylation in embryonic and adult tissues. *Biochim. Biophys. Acta.* 1719:24–35.

Laird, D.W. 2006. Life cycle of connexins in health and disease. *Biochem. J.* 394:527–543.

Lampe, P.D., and A.F. Lau. 2004. The effects of connexin phosphorylation on gap junctional communication. *Int. J. Biochem. Cell Biol.* 36:1171–1186.

Lampe, P.D., W.E. Kurata, B. Warn-Cramer, and A.F. Lau. 1998. Formation of a distinct connexin43 phosphoisoform in mitotic cells is dependent upon $p34^{cdc2}$ kinase. *J. Cell Sci.* 111:833–841.

Lampe, P.D., E.M. TenBroek, J.M. Burt, W.E. Kurata, R.G. Johnson, and A.F. Lau. 2000. Phosphorylation of connexin43 on serine368 by protein kinase C regulates gap junctional communication. *J. Cell Biol.* 149:1503–1512.

Lampe, P.D., C.D. Cooper, T.J. King, and J.M. Burt. 2006. Analysis of Connexin43 phosphorylated at S325, S328 and S330 in normoxic and ischemic heart. *J. Cell Sci.* 119:3435–3442.

Musil, L.S., and D.A. Goodenough. 1991. Biochemical analysis of connexin43 intracellular transport, phosphorylation and assembly into gap junctional plaques. *J. Cell Biol.* 115:1357–1374.

Paznekas, W.A., S.A. Boyadjiev, R.E. Shapiro, O. Daniels, B. Wollnik, C.E. Keegan, J.W. Innis, M.B. Dinulos, C. Christian, M.C. Hannibal, and E.W. Jabs. 2003. Connexin 43 (GJA1) mutations cause the pleiotropic phenotype of oculodentodigital dysplasia. *Am. J. Hum. Genet.* 72:408–418.

Richards, T.S., C.A. Dunn, W.G. Carter, M.L. Usui, J.E. Olerud, and P.D. Lampe. 2004. Protein kinase C spatially and temporally regulates gap junctional communication during human wound repair via phosphorylation of connexin43 on serine368. *J. Cell Biol.* 167:555–562.

Saez, J.C., A.C. Nairn, A.J. Czernik, G.I. Fishman, D.C. Spray, and E.L. Hertzberg. 1997. Phosphorylation of connexin43 and the regulation of neonatal rat cardiac myocyte gap junctions. *J. Mol. Cell. Cardiol.* 29:2131–2145.

Saez, J.C., V.M. Berthoud, M.C. Branes, A.D. Martinez, and E.C. Beyer. 2003. Plasma membrane channels formed by connexins: their regulation and functions. *Physiol. Rev.* 83:1359–1400.

Schulz, R., P. Gres, A. Skyschally, A. Duschin, S. Belosjorow, I. Konietzka, and G. Heusch. 2003. Ischemic preconditioning preserves connexin 43 phosphorylation during sustained ischemia in pig hearts in vivo. *FASEB J.* 17:1355–1357.

Shevchenko, A., M. Wilm, O. Vorm, and M. Mann. 1996. Mass spectrometric sequencing of proteins silver-stained polyacrylamide gels. *Anal. Chem.* 68:850–858.

Sohl, G., and K. Willecke. 2004. Gap junctions and the connexin protein family. *Cardiovasc. Res.* 62:228–232.

Solan, J.L., and P.D. Lampe. 2005. Connexin phosphorylation as a regulatory event linked to gap junction channel assembly. *Biochim. Biophys. Acta.* 1711:154–163.

Solan, J.L., M.D. Fry, E.M. TenBroek, and P.D. Lampe. 2003. Connexin43 phosphorylation at S368 is acute during S and G2/M and in response to protein kinase C activation. *J. Cell Sci.* 116:2203–2211.

Sorgen, P.L., H.S. Duffy, S.M. Cahill, W. Coombs, D.C. Spray, M. Delmar, and M.E. Girvin. 2002. Sequence-specific resonance assignment of the carboxyl terminal domain of Connexin43. *J. Biomol. NMR.* 23:245–246.

Sorgen, P.L., H.S. Duffy, P. Sahoo, W. Coombs, M. Delmar, and D.C. Spray. 2004a. Structural changes in the carboxyl terminus of the gap junction protein connexin43 indicates signaling between binding domains for c-Src and zonula occludens-1. *J. Biol. Chem.* 279:54695–54701.

Sorgen, P.L., H.S. Duffy, D.C. Spray, and M. Delmar. 2004b. pH-dependent dimerization of the carboxyl terminal domain of Cx43. *Biophys. J.* 87:574–581.

Sosinsky, G.E., J.L. Solan, G.M. Gaietta, L. Ngan, G.J. Lee, M.R. Mackey, and P.D. Lampe. 2007. The C-terminus of Connexin43 adopts different conformations in the Golgi and gap junction as detected with structure specific antibodies. *Biochem. J.* 408:375–85.

TenBroek, E.M., P.D. Lampe, J.L. Solan, J.K. Reynhout, and R.G. Johnson. 2001. Ser364 of connexin43 and the upregulation of gap junction assembly by cAMP. *J. Cell Biol.* 155:1307–1318.

White, T., and D. Paul. 1999. Genetic diseases and gene knockouts reveal diverse connexin functions. *Annu. Rev. Physiol.* 61:283–310.

Yi, E.C., H. Lee, R. Aebersold, and D.R. Goodlett. 2003. A microcapillary trap cartridge-microcapillary high-performance liquid chromatography electrospray ionization emitter device capable of peptide tandem mass spectrometry at the attomole level on an ion trap mass spectrometer with automated routine operation. *Rapid Commun. Mass Spectrom.* 17:2093–2098.

Yogo, K., T. Ogawa, M. Akiyama, N. Ishida, and T. Takeya. 2002. Identification and functional analysis of novel phosphorylation sites in Cx43 in rat primary granulosa cells. *FEBS Lett.* 531:132–136.

Yogo, K., T. Ogawa, M. Akiyama, N. Ishida-Kitagawa, H. Sasada, E. Sato, and T. Takeya. 2006. PKA implicated in the phosphorylation of Cx43 induced by stimulation with FSH in rat granulosa cells. *J. Reprod. Dev.* 52:321–328.